



Spatially Resolved Distribution Function and the Medium-Range Order in Metallic Liquid and Glass

SUBJECT AREAS:
CONDENSED MATTER
PHYSICS
MATERIALS PHYSICS
MODELLING AND THEORY
METHODS

X. W. Fang^{1,2}, C. Z. Wang^{1,4,*}, S. G. Hao^{1,4}, M. J. Kramer¹, Y. X. Yao^{1,4}, M. I. Mendeleev¹, Z. J. Ding², R. E. Napolitano^{1,3} & K. M. Ho^{1,4}

¹Ames Laboratory – US Department of Energy, Iowa State University, Ames, Iowa 50011, USA, ²Hefei National Laboratory for Physical Sciences at Microscale and Department of Physics, University of Science and Technology of China, Hefei, Anhui, 230026, P. R. China, ³Department of Materials Science and Engineering, Iowa State University, Ames, IA 50011, USA, ⁴Department of Physics and Astronomy, Iowa State University, Ames, IA 50011, USA.

Received
27 June 2011

Accepted
28 November 2011

Published
23 December 2011

Correspondence and
requests for materials
should be addressed to
C.Z.W. (wangcz@
ameslab.gov)

The structural description of disordered systems has been a longstanding challenge in physical science. We propose an atomic cluster alignment method to reveal the development of three-dimensional topological ordering in a metallic liquid as it undercools to form a glass. By analyzing molecular dynamic (MD) simulation trajectories of a $\text{Cu}_{64.5}\text{Zr}_{35.5}$ alloy, we show that medium-range order (MRO) develops in the liquid as it approaches the glass transition. Specifically, around Cu sites, we observe “Bergman triacontahedron” packing (icosahedron, dodecahedron and icosahedron) that extends out to the fourth shell, forming an interpenetrating backbone network in the glass. The discovery of Bergman-type MRO from our order-mining technique provides unique insights into the topological ordering near the glass transition and the relationship between metallic glasses and quasicrystals.

A correct description of the order parameter in a liquid or glass system is the key to understanding and predicting the dynamics of glass formation and phase selection in undercooled liquid materials. However, the lack of long range order (LRO) in the system introduces a spatially varying rotation between the structural motifs found at different positions in the system making it difficult to discern the details of the developing structural order both in scattering experiments as well as in atomistic simulations^{1–14}. The directional averaging associated with the measurement of simple radial correlations in scattering experiment obscures the angular and species-specific information necessary to quantify the topological and chemical order even in the first coordination shell^{1–5}.

In the analysis of atomistic liquid and glass geometries, although several widely used methods (e.g. Bond-Orientation order¹⁵, Honeycutt-Anderson index^{16,17} and Voronoi tessellation¹⁸) exist to complement the structural information provided by radial-type pair correlations, they suffer from several common deficiencies: (i) They do not provide a visual picture of the structural motifs of the system although some features can be inferred from the numerical statistics provided by these analyses; (ii) They only address structural arrangements in the first coordination shell, extension to characterize medium range order beyond the first shell is not straightforward or, in many cases, non-existent; (iii) They do not treat different structural motifs on an equal footing, which can make comparison between different structural motifs difficult. For example, Voronoi indices can describe icosahedral short range order (ISRO) very well but run into mathematical difficulties when describing fcc-type short range order (SRO); (iv) They provide population statistics but do not provide a quantitative measure of the distance of a given cluster in the system from different competing SRO templates.

In this paper, we propose a robust cluster alignment tool that corrects all of the above deficiencies in existing methods. Our method provides a visual picture of the structural motif as well as a scheme for defining an order parameter to measure the strength of any structural motif at a given locality in the system. The definition of this quantitative order parameter treats all different structural motifs on an equal footing and can be incorporated into modified MD schemes to manipulate the tendencies of the system towards various competing structural motifs. By applying this alignment method to the well-studied $\text{Cu}_{64.5}\text{Zr}_{35.5}$ alloy where the MRO still remains unclear^{8,19–21}, we clearly demonstrate the development of Bergman triacontahedron MRO upon cooling from the liquid state. The discovery of Bergman-type MRO from our order-mining technique provides unique insights into the nature of the glass transition and the relationship between metallic glasses and quasicrystals. Our “order mining” method

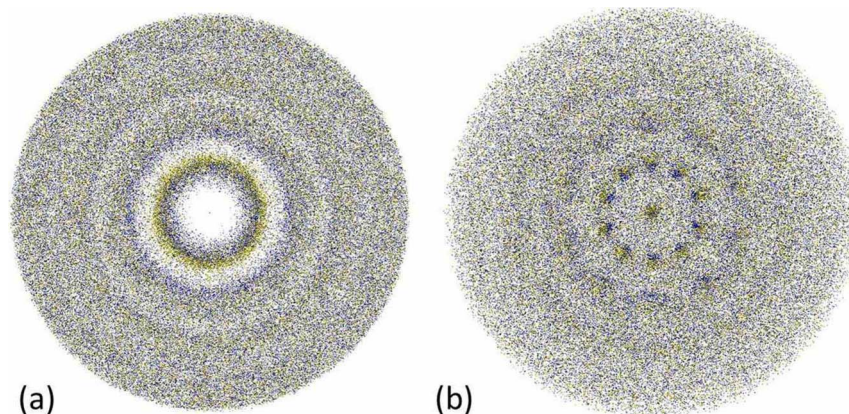


Figure 1 | Atomic distribution of the Cu-centered clusters from the MD simulation of $\text{Cu}_{64.5}\text{Zr}_{35.5}$ at 300K. (a) as-simulated atom positions for 2,000 randomly selected Cu-centered clusters each contains 301 atoms; (b) atom positions after the alignment. For clarity the image is a 2 Å thick slice through the center of the clusters with Cu atoms in blue and Zr atoms in yellow.

is generic and can be used to uncover hidden order in any form of disordered systems including metallic liquids and glasses.

Results

The 3D atomistic structures for both the $\text{Cu}_{64.5}\text{Zr}_{35.5}$ liquid and glass are generated by MD simulations using an accurate interatomic potential based on the Finnis-Sinclair method (FS)²¹. Each structure contains 5000 atoms in a cubic simulation cell, with periodic boundary conditions. The glass structures are generated by cooling from the equilibrated high temperature liquid at essentially zero pressure using a cooling rate as low as 4.91×10^9 K/s. Details about the MD simulations and comparison with scattering experiments are reported elsewhere²². Structures at five temperatures (1500K, 1100K, 900K, 700K and 300K) are used in the present analysis, where the structures at 700K and 300K are below the glass transition temperature which is around 750K²¹.

In order to reveal the development of three-dimensional topological ordering upon cooling in $\text{Cu}_{64.5}\text{Zr}_{35.5}$ liquid and glass, 2000 atomic clusters each of a Cu atom in the center and about 300 atoms around the center atom are randomly picked up from the MD simulation trajectory at each temperature. The 2000 Cu-centered clusters at a given temperature are then aligned with each other to minimize the overall mean square distances among the atoms in different clusters so that the clusters will rotate to have a common orientation. The resulting alignment reveals the inherent structural motif characterizing the local environment of the given chemical constituent. More details about the alignment procedure are given in the methods section and Ref.²².

An example of atomic distribution before and after the alignment is shown in Fig. 1. In this plot, 2000 Cu centered atomic clusters, each consisting of their 300 neighboring atoms, are randomly selected from the trajectory of MD simulation at 300K. Before alignment [Fig. 1(a)], superposition of all clusters translated to a coincident central point, with no rotation, shows that the neighboring atoms are distributed in uniform concentric spheres corresponding to the peaks of the Pair Correlation Function (PCF), with no resolved angular features. After the alignment, however, a clear 10-fold pattern emerges [Fig. 1(b)]. By applying a Gaussian smearing scheme to the 3D atomic distribution after the alignment, a three-dimensional (3D) spatially-resolved distribution function (SRDF)²³ $D(\vec{r})$ can be defined in terms of the relevant 3D position vectors \vec{r} rather than by simple distances as in a typical PCF analysis:

$$D(\vec{r}) = \frac{1}{m} \sum_{i=1}^{m \times n} (\alpha/\pi)^{3/2} e^{-\alpha(\vec{r}-\vec{r}_i)^2} \quad (1)$$

where α is the Gaussian smearing parameter, \vec{r}_i is the position vector of atom i , m is the number of the clusters in the alignment and n is the number of atoms in each cluster.

In Fig. 2, we present the iso-surfaces of the SRDFs for Cu centered clusters in $\text{Cu}_{64.5}\text{Zr}_{35.5}$ at five temperatures obtained from our alignment scheme discussed above. The Cu-centered clusters show that ISRO is already well developed in the liquid at 1500K, which remarkably, is ~ 750 K above T_g . As temperature decreases, the ordering becomes more pronounced as indicated by the increase in sharpness and intensity of the iso-surfaces. It is also clear that the icosahedral order gradually extends outward with decreasing temperature with

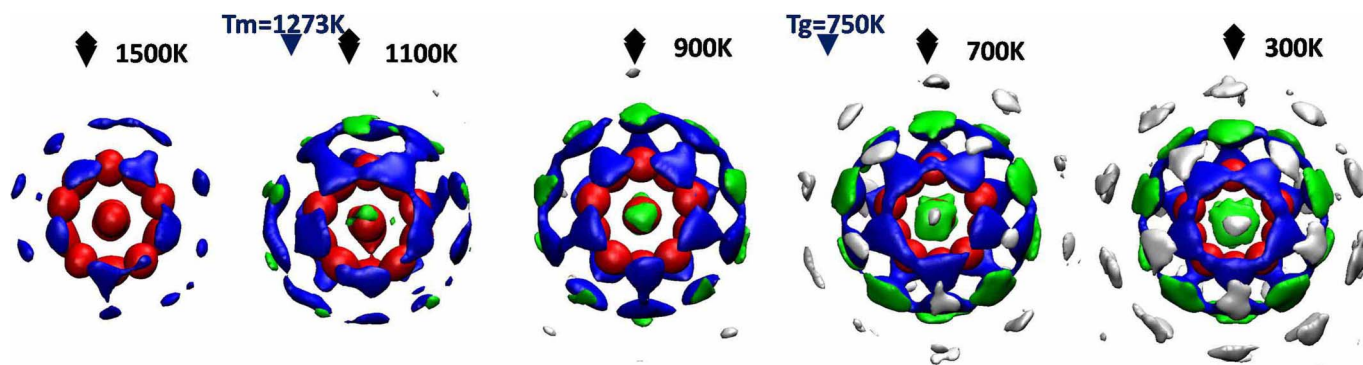


Figure 2 | Cu-centered SRDF at different temperatures (iso value : 0.081 \AA^{-3}). T_m and T_g are the melting point and the glass transition temperatures, respectively. Different colors are used here to indicate different coordination shells: red (first shell, icosahedron), blue (second shell, dodecahedron), green (third shell, icosahedron), and white (fourth shell, rhombic triacontrahedron). The parameter α is chosen to be 4.0 \AA^{-2} to obtain optimal smoothness and resolution in the SRDF, but the resultant SRDF is not very sensitive to this parameter. The MRO at 300K can be seen to extend up to $\sim 15 \text{ \AA}$.



iso-surfaces clearly discernable out to as far as the fourth shell for the glass at 300 K.

To quantify the SRO and MRO, we examine the intensities of individual peaks in the SRDF in each shell of the Cu-center cluster at four different temperatures. Fig. 3(b) shows the peak intensities at different temperatures averaged over all peaks in a given shell and normalized by $D(\vec{r}=0)$. The vertical bars in this figure indicate the variation of peak intensities within a given shell. Smaller variance at lower temperatures indicates stronger and more uniform icosahedral ordering. To obtain a characteristic decay length d for the icosahedral order at different temperatures, the directionally averaged peak intensities were fitted to an exponential decay function, $I = e^{-r/d}$, where r is the radius of a given shell in the SRDF (Fig. 3 and insert table). This provides a quantitative measure of the degree of ordering in this alloy. At lower temperatures, the decay length d increases due to increasing local order at longer lengths (Fig. 2). In the present analysis, the chemical identities of the atoms were not considered, but the extension of the analysis to obtain partial distributions is straightforward and is expected to yield insight into the chemical ordering in the system.

Discussion

Results from both scattering experiment and MD simulations both indicate a splitting in the second peak of the PCF in the $\text{Cu}_{64.5}\text{Zr}_{35.5}$ system when cooling from the liquid to a glass²⁴. This well-known splitting has been the subject of some speculation in the past⁴ but there is as yet no firm evidence of the physical origin of this effect. The SRDF can be used to clearly identify the origin of this behavior⁴. Overlaying the atom positions for part of a Bergman triacontahedron cluster²⁵ along the 3-fold direction over the SRDF, one can easily identify the icosahedral-dodecahedral-icosahedral arrangement around the Cu center. Fig. 3(c) shows the Cu-centered partial PCF at different temperatures, where it is very clear that the second peak tends to split into two adjacent peaks (i.e. a right shoulder of the second peak develops) as temperature decreases. Our SRDF analysis reveals that

the structural changes associated with the increasing second-peak shoulder corresponds to the development of strong ordering in the third coordination shell (green atoms in the Bergman model of Fig. 3(c)) below T_g . This illustrates the utility of the cluster alignment scheme and the SRDF analysis, with which we can map the PCF into real space, thereby recovering the angular components of the radial distribution function.

Finally, we also note that while the first shell 13-atom icosahedral clusters are readily formed in the liquid at high temperatures, Bergman-type MRO only develops near T_g . We examine the population and distribution of the Bergman-type clusters as the function of temperature. The atomic coordinates averaged over 200 successive MD snapshots at each temperature are used for the analysis in order to remove the effects from the thermal motions. The distribution of the Bergman-type clusters in the whole sample at 900, 700 and 300K are plotted in Fig. 4. At 900K, there are only some isolated Bergman-type clusters in the system (Fig. 4 (a)). Below T_g , a much higher density of bergman clusters is observed, forming a backbone network at 700 and 300K (Fig. 4 (b) and (c)). The clear emergence of a Bergman-type cluster network in the metallic glass suggests a possible connection between the atomistic structures of metallic glasses and quasicrystals based on building blocks of Bergman clusters^{25,26}. In the quasicrystal, the Bergman clusters are well oriented and have long range rotational order. While in metallic glasses, the orientation correlation between individual Bergman-type clusters is much weaker. The similarities and differences between the quasicrystals and metallic glasses may also give a clue to understanding why small variations in the chemical composition can alter the structure and formability of quasicrystal and metallic glass. For a given system, the chemical composition of the Bergman clusters should be similar and fixed more or less by the SRO in the system. However, additional small changes in the overall chemical composition can result in significant changes in the composition for the atoms in the glue region between the Bergman clusters and alter the spatial cluster-packing in favor or disfavor of phase ordering among the Bergman clusters.

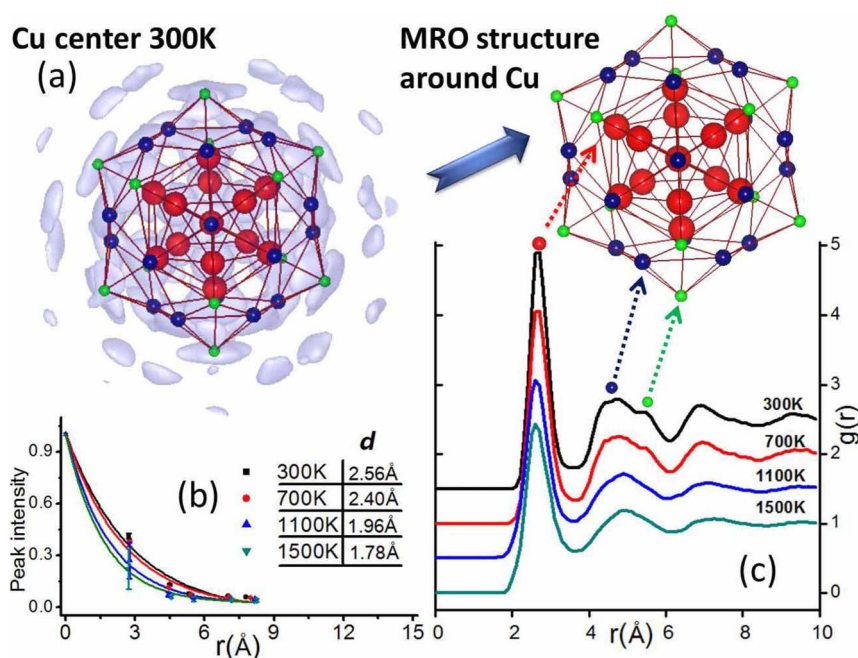


Figure 3 | A summary of the Cu-centered MRO at 300K. (a) SRDF (blue isosurface (0.081 \AA^{-3}), with local maxima shown as embedded spheres (Color represents different shells: red = 1st, blue = 2nd, green = 3rd.); (b) radial decay of local maxima, averaged over each individual shell and normalized by the intensity at $r=0$, shown with exponential fit (The inset table shows the fitted decay lengths.); (c) correspondence between MRO structure and conventional Cu-Centered partial PCF: first shell (red spheres) to the first PCF peak, second shell (blue spheres) to the second PCF peak, and third shell (green spheres) to the developing third PCF peak.

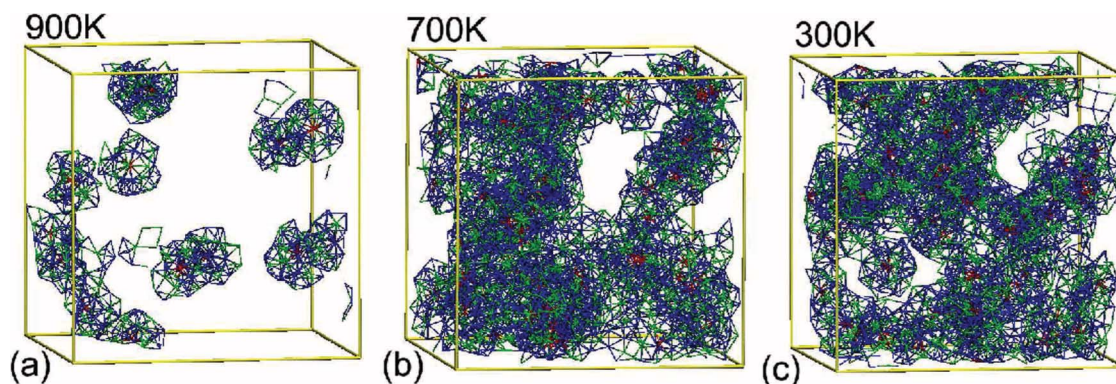


Figure 4 | Development of Bergman triacontahedral clusters as the temperature is decreased. (a) 900K, 14 Bergman triacontahedral clusters which contain 12.1% of atoms; (b) 700K, 89 Bergman triacontahedral clusters which contain 46.9% of atoms; (c) 300K, 79 Bergman triacontahedral clusters which contain 44.8% atoms in the whole sample. The Cu atoms are in blue, Zr in green and the center atoms of the Bergman triacontahedral clusters are in red. The population of the Bergman-type clusters is analyzed using the atomic coordinates averaged over 200 successive MD snapshots at each temperature to remove the effects from the thermal motions. The difference in the population of the Bergman-type clusters at 700 and 300K is partially due to the cooling from different initial configurations in the MD simulations.

In summary, we provide a direct “order mining” tool that can be used to map out the SRDF, revealing and quantifying various aspects of MRO in noncrystalline systems which have remained poorly resolved with other analytic methods. We have applied the method to characterize the MRO that develops in $\text{Cu}_{64.5}\text{Zr}_{35.5}$ alloy as temperature decreases. We show that Bergman-type MRO and a backbone network of interpenetrating Bergman-type clusters develop as the system approaches the glass transition. The discovery of Bergman triacontahedron MRO in the metallic glass sheds interesting light on the nature of the glass transition. In particular, it provides useful clues for understanding the kinetic pathway for slowing down the dynamics of the system and driving the system into non-ergodic behavior and the structural relation between metallic glasses and quasicrystals. Identification of these long range structural motifs also allow us to examine the influence of changing stoichiometry on the free energy competition between non-crystalline and various crystalline motifs and hopefully understand the chemical influence on glass formation tendency. In addition to giving detailed description of the structural motifs developing in the system, the order parameters obtained from such an “order mining” procedure can be incorporated into MD simulation (e.g., as collective variable in metadynamics) to overcome time-scale limitations in MD simulation of metallic liquid and glass systems.

Methods

In our alignment scheme, we characterize the local environment of each atom in the sample by an atomic cluster which includes the atom itself and its neighbors. The total number of such clusters is equal to the number of atoms in the sample. For binary alloys, we divide the clusters into subsets according to the chemical constituent of the center atom. The clusters in the same subset (according to the chemical constituent of the center atom) are aligned with each other to minimize the overall mean square distances between different clusters. The clusters are rigidly rotated and translated relatively to each other during the alignment. To carry out this alignment, a simulated annealing scheme implemented with molecular dynamics (MD) simulation is employed. The results of this alignment will reveal the common structural motif characterizing the local environment of a given chemical constituent. The use of the MD scheme permits the alignments of all the clusters in the subsets to be done simultaneously to obtain a consensus motif in an efficient manner.

In the MD alignment simulations a modified Lenard-Jones type attractive potential is used to describe the attractive interaction between the atoms in different local clusters.

$$V_{i,j,m}(r) = -0.04 \times \varepsilon \times \left(\frac{\sigma^2}{r_{i,j,m}^2 + \Delta} \right)^3 \quad (2)$$

where $V_{i,j,m}$ is the attractive potential between atom m in cluster i and atom n in cluster j ($i \neq j$), and $r_{i,j,m}$ is the distance between atom m in cluster i and atom n in cluster j . The cutoff distance for the attractive interaction $V_{i,j,m}$ is set to be 1.0σ , and the parameter in Equation (2) is set to $0.5\sigma^2$.

A strong harmonic potential is also introduced between atom pairs within the same cluster to keep the structure quasi-rigid during the collective-alignment process.

$$U_{m,n} = -\frac{1}{2}K \times (r_{m,n} - r_{m,n}^0)^2 \quad (3)$$

where $U_{m,n}$ is the strong harmonic potential between atom m and atom n , and the $r_{m,n}$ is the distance between atom m and atom n in the same cluster. $r_{m,n}^0$ is the initial distance between atom m and n before alignment. A force constant $K = 4.0 \times 10^4 \text{ eV}/\sigma^2$ is large enough to guarantee that the geometric distortions of each cluster during the alignment are negligible.

Although in principle all the clusters in a subset can be used in the collective-alignment, we find that 2000 local clusters randomly selected from each subset provide sufficient statistical sampling of the SRO in liquids and glasses. We also find that the alignments can be done more efficiently by first performing the alignment simulation on the small clusters involving only the first shell atoms, and then extend the alignment to further outer shells using the rotation matrices of the clusters determined from the first shell alignment.

- Hufnagel, T. C. Amorphous Materials: Finding order in disorder. *Nature materials* **3**, 666–667 (2004).
- Treacy, M. M. J. & Gibson, J. M. Variable Coherence Microscopy: a Rich Source of Structural Information from Disordered Materials. *Acta Cryst.* **A52**, 212–220 (1996).
- Hirotsu, Y., Ohkubo, T. & Matsushita, M. Study of amorphous alloy structures with medium range atomic ordering. *Microsc. Res. Techniq.* **40**, 284–312 (1998).
- Kelton, K. F., Lee, G. W., Gangopadhyay, A. Y., Hyers, R. W., Rathz, T. J., Rogers, J. R., Robinson, M. B., & Robinson, D. S. First X-Ray Scattering Studies on Electrostatically Levitated Metallic Liquids: Demonstrated Influence of Local Icosahedral Order on the Nucleation Barrier. *Phys. Rev. Lett.* **90**, 195504 (2003).
- Saida, J., Matsushita, M. & Inoue, A. Direct observation of icosahedral cluster in $\text{Zr}_{70}\text{Pd}_{30}$ binary glassy alloy. *Appl. Phys. Lett.* **79**, 412. (2001).
- Sheng, H. W., Luo, W. K., Alamgir, F. M., Bai, J. M. & Ma, E. Atomic packing and short-to-medium-range order in metallic glasses. *Nature* **439**, 419 (2006).
- Miracle, D. B. A structural model for metallic glasses. *Nature Materials* **3**, 697–702 (2004).
- Li, M. Z., Wang, C. Z., Hao, S. G., Kramer, M. J. & Ho, K. M. Structural heterogeneity and medium-range order in $\text{Zr}_x\text{Cu}_{100-x}$ metallic glasses. *Phys. Rev. B* **80**, 184201 (2009)
- Wang, S. Y. *et al.* Short- and medium-range order in a $\text{Zr}_{73}\text{Pt}_{27}$ glass Experimental and simulation studies. *Phys. Rev. B* **78**, 184204 (2008).
- Elliott, S. R. Medium-range structural order in covalent amorphous solids. *Nature*, **354**, 445 (1991).
- Schenk, T., Holland-Moritz, D., Simonet, V., Bellissent, R., & Herlach, D. M. Icosahedral Short-Range Order in Deeply Undercooled Metallic Melts. *Phys. Rev. Lett.* **89**, 075507 (2002).
- Luo, W. K., Sheng, H. W., Alamgir, F. M., Bai, J. M. He, J. H. & Ma, E. Icosahedral Short-Range Order in Amorphous Alloys. *Phys. Rev. Lett.* **92**, 145502 (2004).
- Saksl, K. *et al.* Evidence of icosahedral short-range order in $\text{Zr}_{70}\text{Cu}_{30}$ and $\text{Zr}_{70}\text{Cu}_{29}\text{Pd}_1$ metallic glasses. *Appl. Phys. Lett.* **83**, 3924. (2003).



14. Zhang, L., Wu, Y. S., Bian, X. F., Li, H., Wang, W. M., Wu, S. Short-range and medium-range order in liquid and amorphous $\text{Al}_{90}\text{Fe}_5\text{Ce}_5$ alloys. *J. Non-Cryst. Solids*, **262**, 169–176 (2000).
15. Steinhardt, P. J., Nelson, D. R. & Ronchetti, M. Bond-orientational order in liquids and glass. *Phys. Rev. B* **28**, 784 (1983).
16. Honeycutt, J. D. & Andersen, H. C. Molecular dynamics study of melting and freezing of small Lennard-Jones clusters. *J. Phys. Chem.* **91**, 4950 (1987).
17. Ganesh, P. & Widom, M. Signature of nearly icosahedral structures in liquid and supercooled liquid copper. *Phys. Rev. B* **74**, 134205 (2006).
18. Finney, J. L. Modelling the structures of amorphous metals and alloys. *Nature* **266**, 309 (1977); Finney, J. L. *Random packing and the structure of simple liquids*. *Proc. R. Soc. A* **319**, 479 (1970).
19. Wang, X. D., Yin, S., Cao, Q. P., Jiang, J. Z., Franz, H. & Jin, Z. H. Atomic structure of binary $\text{Cu}_{64.5}\text{Zr}_{35.5}$ bulk metallic glass. *Appl. Phys. Lett.* **92**, 011902 (2008).
20. Cheng, Y. Q., Sheng, H. W. & Ma, E. Relationship between structure, dynamics, and mechanical properties in metallic glass-forming alloys. *Phys. Rev. B* **78**, 014207 (2008).
21. Mendelev, M. I., Kramer, M. J., Ott, R. T., Sordelet, D. J., Yagodin, D. & Popel, P. Development of suitable interatomic potentials for simulation of liquid and amorphous Cu-Zr alloys. *Philos. Mag.* **89**, 967–987 (2009).
22. Fang, X. W., Wang, C. Z., Yao, Y. X., Ding, Z. J. & Ho, K. M. Atomistic Cluster Alignment Method for Local Order Mining in Liquids and Glasses. *Phys. Rev. B* **82**, 184204 (2010).
23. Kusalik, P. G. & Svishchev, I. M. *The Spatial Structure in Liquid Water*. Science, **265**, 1215 (1994).
24. Mendelev, M. I. *et al.* Experimental and computer simulation determination of the structural changes occurring through the liquid-glass transition in Cu-Zr alloys. *Philos. Mag.* **90**, 3795–3815 (2010).
25. Bergman, G., Waugh, J. L. T. & Pauling, L. The crystal structure of the metallic phase $\text{Mg}_{32}(\text{Al}, \text{Zn})_{49}$. *Acta Cryst.* **10**, 254 (1957).
26. Lin, Q. & Corbett, J. D. A Chemical Approach to the Discovery of Quasicrystals and Their Approximant Crystals. *Springer-Verlag, Berlin*, **133**, 1–39 (2009).

Acknowledgement

We thank Prof. Alan Goldman for useful discussion and critical reading of the manuscript. This work was supported by Basic Energy Sciences, Office of Science, U.S. Department of Energy, under Contract No. DE-AC02-07CH11358. Support including a grant for computer time at the National Energy Research Supercomputing Center (NERSC) in Berkeley, CA. X. W. Fang acknowledges the support from China Scholarship Council for the Postgraduate Scholarship Program (File NO.2008634035) and Z. J. Ding acknowledges the National Natural Science Foundation of China (Grant No.~10874160) and the '111' project.

Author contribution

K. H., C.W., X. F., M. K., and R. N. conceived and designed the research and analysis. X. F., C. W., Y. Y., Z. D., and K. H. developed the cluster alignment method. M. M. performed the molecular dynamics simulation. X. F., C. W., S. H., K. H., performed the analysis. C. W., X. F., S. H., M. K., K. H., and R. N. co-wrote the paper. All authors discussed the results and revised on the manuscript.

Additional information

Competing financial interests: The authors declare no competing financial interests.

License: This work is licensed under a Creative Commons Attribution-NonCommercial-ShareAlike 3.0 Unported License. To view a copy of this license, visit <http://creativecommons.org/licenses/by-nc-sa/3.0/>

How to cite this article: Fang, X.W. *et al.* Spatially Resolved Distribution Function and the Medium-Range Order in Metallic Liquid and Glass. *Sci. Rep.* **1**, 194; DOI:10.1038/srep00194 (2011).